Journal of Power Sources 185 (2008) 1009–1014

Contents lists available at ScienceDirect

Journal of Power Sources

journal homepage: www.elsevier.com/locate/jpowsour

Flow distribution in parallel-channel plate for proton exchange membrane fuel cells

Xiao Yu[a,b], Ming Pingwen[c,*], Hou Ming[a], Fu Yunfeng[c], Yi Baolian[a], Zhi-Gang Shao[a]

[a] Dalian Institute of Chemical Physics, Dalian 116023, Liaoning, China
[b] Chinese Academy of Sciences, Dalian 116023, Liaoning, China
[c] Dalian Sunrise Power Co., Ltd., Dalian 116025, Liaoning, China

ARTICLE INFO

Article history:
Received 15 July 2008
Received in revised form 31 August 2008
Accepted 1 September 2008
Available online 18 September 2008

Keywords:
Fuel cell
Manifold opening
Flow distribution
Model
Parallel channel

ABSTRACT

Parallel channel flow field with manifold openings is widely used in Proton exchange membrane fuel cells (PEMFCs) because of its low-pressure drop and easiness of manufacture. This research presents a hydrodynamic model to describe the airflow distribution, and the predicted pressure differences are validated by experiments. We also investigate the influences of the flow rate, the geometry of header and the length ratio of manifold opening to header region on the airflow distribution. Therefore, the optimal strategy is proposed based on an overall consideration of uniformity and configuration in the fuel-cell plate for application.

1. Introduction

Proton exchange membrane fuel cells (PEMFCs) are considered as the most promising energy conversion systems for vehicles and station applications in the future [1]. However, many of the fundamental processes are only partially understood, and the configuration of the gas-distribution plate is one of the key issues that impact the commercialization process. The flow field should be easier for gas transport with less pressure drop and can maintain uniform flow across the surface of the electrode.

Recently, many channel configurations of distributor plates have been studied, such as parallel [2–4], serpentine [5,6] and interdigitated [7] channels. As for the parallel-channel plate, the design of header configuration is quite important. Former researchers often concentrate on the Z- and U-type configurations, which have been solved with hydrodynamic models or CFD simulations [8]. In practice, the parallel-channel plates with manifold openings [9] (see Fig. 1) are often used to avoid overmuch pressure drop and obtain uniform flow distribution. However, there are few models to describe the flow distribution in such configuration. As a matter of experience, the length ratio of manifold opening to header region can greatly influence the flow distribution in the plate, thus, the reasonable value should be discussed to assist the designer.

It is the purpose of this paper to provide a simple hydrodynamic model for the flow distribution in the parallel-channel plate with manifold openings. The experimental studies are also given to validate the pressure difference distribution in such small size of these channels. In this way, the key factors that affect the flow distribution will be found. Especially, the length ratio of manifold opening to header region is considered. Therefore, the optimal strategy for both uniform distribution and compact construction is discussed below.

2. Model description

2.1. Flow distribution in a gas-distributor plate

The flow pattern in the parallel-channel plate with manifold openings is depicted in Fig. 2. All the parallel channels are separated by ribs and numbered in sequence. There are N discrete channels in the plate; consequently, the header region can be discretized on a mesh of N nodes, and the manifold openings cover N_b of the total N channels in both inlet and outlet. The gas enters from the inlet manifold opening and flows though individual channels via the feed header region, then converges at the outlet distribution region and leaves the plate from the outlet manifold opening. The volume flow rate in each of N individual channels is denoted by q_x (i). Thus, in

* Corresponding author. Tel.: +86 411 84753000; fax: +86 411 84379185.
E-mail address: pwming@dicp.ac.cn (P. Ming).

0378-7753/$ – see front matter © 2008 Elsevier B.V. All rights reserved.
doi:10.1016/j.jpowsour.2008.09.015

Nomenclature

List of symbols

A	cross-section area (m^2)
d	width (m)
D	hydraulic diameter (m)
err	error
f	friction factor
F_y	force exerted on control volume (N)
h	height (m)
L	length (m)
M	mass flow rate ($kg\,s^{-1}$)
N	number of channels
N_b	number of channels covered by the manifold opening
P	perimeter (m)
P_{in}	pressure at the beginning of the channel (Pa)
P_{out}	pressure at the end of the channel (Pa)
q_x	volume flow rate through each channel ($m^3\,s^{-1}$)
Q	cumulative volume flow rate ($m^3\,s^{-1}$)
u_x	mean velocity in the channel ($m\,s^{-1}$)

Greek letters

α	aspect ratio
μ	air viscosity (Pa s)
ρ	air density ($kg\,m^{-3}$)
τ	shear stress ($N\,m^{-2}$)
Φ	characteristic parameter ($kg\,m^{-3}\,s^{-1}$)
Ψ	non-dimensional geometry parameter

Subscripts

in	near the inlet side
out	near the outlet side
x	direction along the channel
y	direction along the header
0	standard situations

the inlet distribution region, the cumulative volume flow rate ($Q_{in}(i)$) is defined as

$$Q_{in}(i) = \sum_{j=1}^{i-1} q_x(j) = Q_{in}(i-1) + q_x(i-1), \quad (i = 2,\ 3, \ldots, N - N_b) \tag{1}$$

$$Q_{in}(1) = 0 \tag{2}$$

In the inlet manifold opening, the mass balance equation can be written as

$$Q_{IN} = \sum_{j=1}^{N} q_x(j) = \sum_{j=N-N_b}^{N} q_x(j) + Q_{in}(N - N_b) \tag{3}$$

where Q_{IN} is the total feed volume flow rate, while in the outlet distribution region, the similar variables are given by

$$Q_{out}(i) = \sum_{j=i}^{N} q_x(j) = Q_{out}(i+1) + q_x(i),$$

$$(i = N_b + 1, N_b + 2, \ldots, N - 1) \tag{4}$$

$$Q_{out}(N) = q_x(N) \tag{5}$$

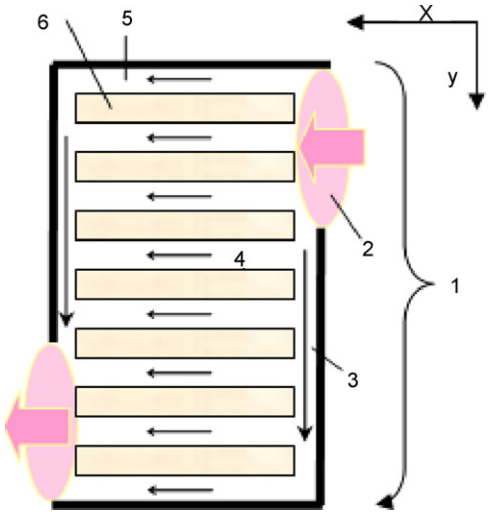

Fig. 1. Schematic diagram of parallel-channel plate with manifold openings in the header region. (1) Header region, (2) manifold opening, (3) distribution region, (4) flow field region, (5) channel and (6) rib.

In the outlet manifold opening, the mass balance equation becomes:

$$Q_{OUT} = \sum_{j=1}^{N_b} q_x(j) + Q_{out}(N_b + 1) \tag{6}$$

Because we suppose there is neither electrochemical reaction nor leakage in the flow field, the Eqs. (3) and (6) are equal.

2.2. Steady channel flow with lower Re

Now, the flow distribution in the plate can be obtained, and the flow rate through each channel is governed by the pressure difference between the beginning and end of the channel, which is expressed as $P_{in}(i)$ minus $P_{out}(i)$. For steady Hagen–Poiseuille flow in a channel, the net pressure balances the force caused by the shear stress at the wall:

$$(P_{in}(i) - P_{out}(i))A_x = \tau_x P_x L_x \tag{7}$$

where A_x is the channel cross-section area, P_x is the channel perimeter, and L_x is the length of the channel. The shear stress (τ_x) is usually expressed in terms of the friction factor f_x.

$$f_x = \frac{\tau_x}{1/2\rho u_x(i)^2} \tag{8}$$

where $u_x(i)$ is the mean velocity in the channel, and the friction factor is a function of the Reynolds number:

$$Re_x = \frac{\rho D_x u_x(i)}{\mu} \tag{9}$$

where D_x represents the hydraulic diameter, and is defined as

$$D_x = \frac{4A_x}{P_x} \tag{10}$$

By the empirical correlation of Kays and Crawford [10], the $(Ref)_x$ depends on the channel aspect ratio ($\alpha_x = d_x/h_x$), hence:

$$(Ref)_x \approx 13.74 + 10.38 \exp\left(\frac{-3.4}{\alpha_x}\right) \tag{11}$$

From Eqs. (7)–(10), the pressure difference from the inlet to the outlet is described as

$$P_{in}(i) - P_{out}(i) = \Phi_x L_x u_x(i) \tag{12}$$

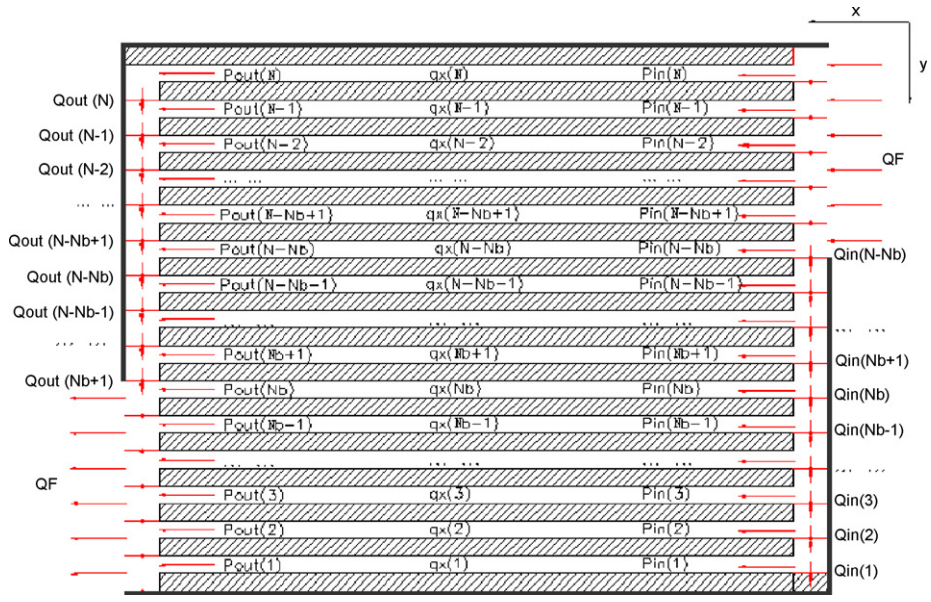

Fig. 2. Illustration of the flow distribution and mesh network in a fuel-cell plate with manifold openings.

here

$$\Phi_x = \mu \frac{2(Ref)_x}{D_x^2} \tag{13}$$

Then the pressure difference from each channel can be obtained directly from the linear flow velocity ($u_x(i)$) in the corresponding channel.

2.3. Pressure distribution in header regions

Derivation of the momentum equation is formulated for a suitable control volume located in the outlet distribution region, as shown in Fig. 3. For one-dimensional axial flow, the momentum balance is stated as

$$\int_{CV} \left(\frac{\partial \rho u_y}{\partial t} + \frac{\partial (\rho u_y u_y)}{\partial y} \right) dV = \sum F_y \tag{14}$$

where F_y is a force exerted on this volume and is composed of two forces: one is due to normal stress on the cross-sectional flow area, as the first integral on the right-hand side in Eq. (15); the other is derived from viscous drag at the channel walls. Restricting attention to the steady flow:

$$\int_{CV} \frac{\partial (\rho u_y u_y)}{\partial y} dV = \int_{CS} \tau_y \vec{n}\, dA_y - \int_{CS} \tau_y dA_y \tag{15}$$

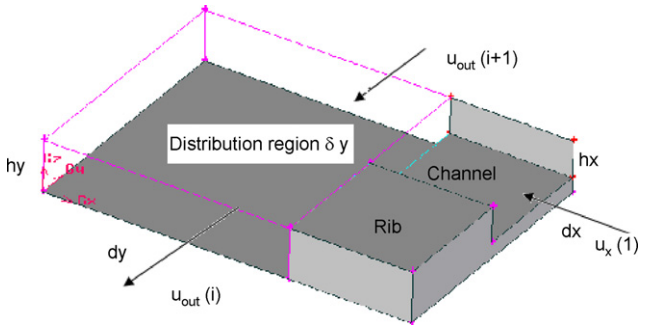

Fig. 3. Control volume for a section in the outlet distribution region.

With the help of Gauss divergence theorem, the first integral on the right-hand side converts to a volume integral. The shear drag term can be rewritten in one dimension:

$$\int_{CV} \frac{\partial (\rho u_y u_y)}{\partial y} dV = \int_{CV} (\nabla \cdot \tau_y) dA_y - \int_y \tau_y P_y dy \tag{16}$$

where P_y is the perimeter of the distribution region, and A_y is the crossing-section area. τ_y is the normal stress, which depends on the pressure drop. Shrinking the control volume, the desired differential equation can be expressed as

$$\frac{d(\rho u_y u_y)}{dy} = -\frac{dp}{dy} - \frac{P_y}{A_y} \tau_y \tag{17}$$

Similar to the channel flow, the wall stress is determined in terms of a friction factor f_y, which depends on the header dimensions and fluid properties. Assuming the properties are constant, for an incompressible flow, the momentum equation can be rewritten as

$$2\rho u_y \frac{du_y}{dy} + \frac{dp_y}{dy} + \Phi_y u_y = 0 \tag{18}$$

here

$$\Phi_y = \mu \frac{2(Ref)_y}{D_y^2} \tag{19}$$

The subscript y = out refers to the exhaust header region and y = in refers to the feed header region.

Because there are a discrete number of channels, it is appropriate to represent and solve the momentum equations in discrete form. As shown in Fig. 3, the control volume in the outlet distribution region is taken as rectangular, with the height h_y and the width d_y. Since the differential equation is first-order and the boundary conditions should be satisfied, it is appropriate to forward difference this equation.

$$P_{out}(i+1) - P_{out}(i) = -2\rho u_{out}(i)(u_{out}(i+1) - u_{out}(i))\,\delta y - \left(\mu \frac{2(Ref)_y}{D_y^2} \right) u_{out}(i)\,\delta y, \quad (i = N_b, N_b+1, \ldots, N-1) \tag{20}$$

where $u_{out}(i)$ can be obtained from the flow distribution in Section 2.1:

$$u_{out}(i) = \frac{Q_{out}(i)}{A_y}, \quad (i = 1, 2, \ldots, N) \tag{21}$$

Specifically, for the outlet manifold opening:

$$P_{out}(i) = P_{exit}, \quad (i = 1,\ 2, \ldots,\ N_b) \tag{22}$$

Similarly, for the inlet manifold opening:

$$P_{in}(i) = P_{IN}, \quad (i = N - N_b,\ N - N_b + 1, \ldots, N) \tag{23}$$

However, the sense of the difference in the feed header region is opposite that of the exhaust header:

$$P_{in}(i) - P_{in}(i-1) = -2\rho u_{in}(i-1)(u_{in}(i) - u_{in}(i-1))\,\delta y - \left(\mu \frac{2(Ref)_y}{D_y^2}\right) u_{in}(i-1)\,\delta y, \quad (i = 2,\ 3, \ldots, N - N_b) \tag{24}$$

here

$$u_{in}(i) = \frac{Q_{in}(i)}{A_y}, \quad (i = 1, 2, \ldots, N) \tag{25}$$

2.4. Solution algorithm

The program layout is shown in Fig. 4, and this calculation starts with an initially guessed set of channel volume flow rates, $q_x(i)$. Then the cumulative flow rates in the headers, $Q_{in}(i)$ and $Q_{out}(i)$, $u_{out}(i)$ and $u_{in}(i)$, can be obtained from the Eqs. (1), (4), (21), and (25). These velocities are used to calculate the pressures in header regions. The next step is to calculate the corresponding flow rates in the channel, $u_{x\_new}(i)$ and $q_{x\_new}(i)$, from the Eqs. (12) and (13). Of course, the new value of flow rates should be adjusted first.

$$q_{x\_new}^{adj}(i) = \frac{Q_{IN}}{\sum_{i=1}^{N} q_{x\_new}(i)} q_{x\_new}(i) \tag{26}$$

At last, the accumulate error has to be compared with the set precision.

$$err = \sum_{i=1}^{N} \left[\frac{q_{x\_new}^{adj}(i) - q_x(i)}{q_x(i)}\right]^2 \tag{27}$$

The program will keep on running with a new set of channel flow rates until all the flow rates are close to the old ones within the error limit.

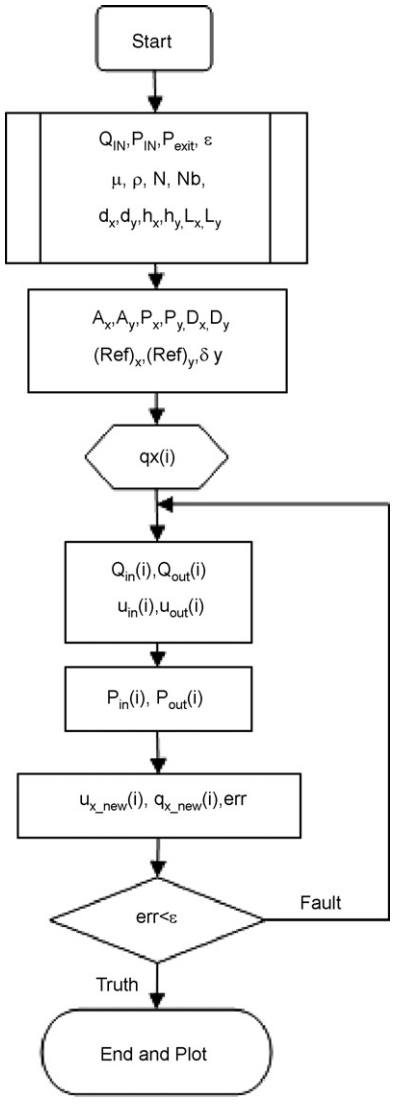

Fig. 4. The program layout for flow distribution calculation.

3. Experimental

In order to validate the flow distribution in the parallel-channel plate, a fine facility was used as shown in Fig. 5. The transparent separator was made of PMMA (polymethyl methacrylate), of which 62 pairs of little holes were punched out along the edge in two rows. The controlled airflow entered from the inlet manifold opening, and this certain amount flow was achieved by the mass flow controller (D07-19A). Also the pressure drop along each channel could be measured from the corresponding pair of holes in the separator. In order to avoid the edge effect, these holes were kept a certain distance away from the inlet or outlet. So the test length of the channel was 275 mm of the whole 358 mm, and the experimental data should be enlarged proportionally. Two pressure transducers were used for pressure measurements over the range of 0–3 kPa (STD110 Honeywell) and 0–20 kPa (STD930 Honeywell) with 0.065% full-scale accuracy for both. In this way, any pressure difference between the beginning and end of the channel would be received. The operation was kept in room temperature and other parameters of the set-up were described in Table 1.

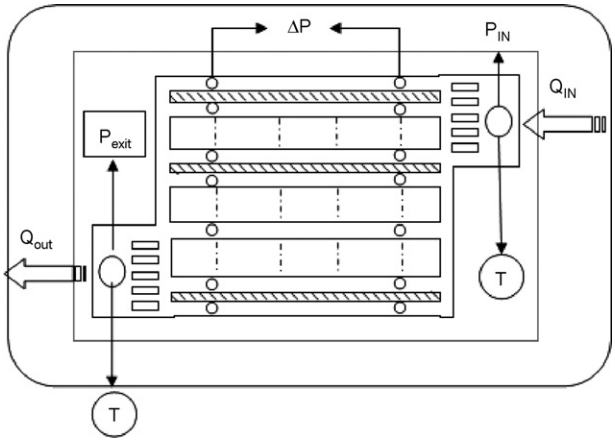

Fig. 5. Illustration of the facility with 62 pairs of holes for pressure difference measurement in each channel.

Table 1
Specification of the flow field configuration and operating conditions.

Variable	Units	Value
Number of channels	–	62
Total length of the header region	mm	90
Length of the channel	mm	356
Room temperature	°C	20
Air density	kg m^{-3}	1.293
Air viscosity	Pa s	1.72×10^{-5}
Standard mass flow rate	kg s^{-1}	2.16×10^{-5}

Table 2
Experimental cases and the corresponding parameters.

Case description	Volume flow rate (sccm)	Total pressure drop (kPa)	Ψ_x	Ψ_y
#1	1000	5.77	8.68	5.51
#2	4000	21.0	8.68	5.51
#3	6000	31.0	8.68	5.51
#4	1000	2.59	7.97	3.78

4. Results and discussion

4.1. Pressure differences and flow distribution

In this study, four experiments under different conditions are listed in Table 2. In case 4, the volume flow rate of the air was 1000 sccm, with the inlet and outlet pressure 2.83 and 0.24 kPa, respectively. Comparing with the model prediction in Fig. 6(a), the measured pressure differences in the parallel plate are indicated as stars. From Eq. (12), the flow rate has a liner relationship with the pressure difference in each channel. Thus, the corresponding flow distribution map is drawn in Fig. 6(b). Along the numbered channel, the maximum volume flow rate is acquired at the 29th channel, which is 16.6 sccm. By contrast, the minimum value lies at the edge of the gas-distributor plate, which is 15.9 sccm in the 1st and Nth channel.

4.2. Effect of feed flow rate on flow distribution

For a fixed fuel cell (Cases 1–3 in Table 2), the feed volume flow rate determined the total inlet and outlet pressure, which could be measured in situ. In this experimental set-up, the stable pressure differences of all the channels could be detected and compared with the model's prediction. As shown in Fig. 7(a), the predicted curves

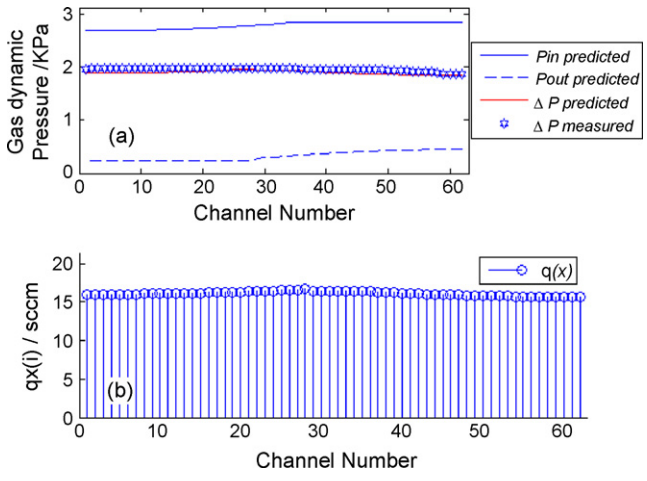

Fig. 6. (a) Validate the pressure difference distribution and (b) show the corresponding flow rate distribution in the parallel-channel plate.

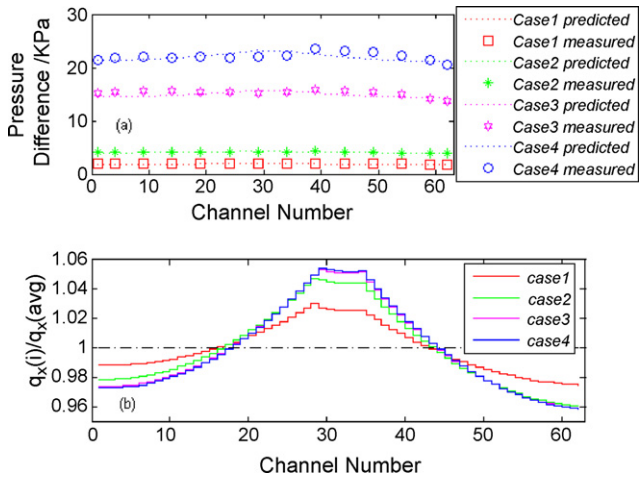

Fig. 7. (a) Compare the effect of different flow rates on the pressure difference distribution by model prediction and experimental measurement, and then (b) show the corresponding ratio of flow rate distribution map.

of pressure difference are plotted against the number of channels for various feed flow rates, and they were also validated by experiments. It is found that the non-uniformity in the flow distribution increases with the flow rate. In this configuration, the minimum flow rate lies at the edge of the plate, and the highest mass flow usually exists near the centre (see Fig. 7(b)).

4.3. Two characteristic parameters

With the objective of generalizing the results, the characteristic parameters in Eqs. (13) and (19) can be recast in terms of non-dimensional parameters:

$$\Psi_x = \frac{\Phi_x L_x A_x}{M_0} \tag{28}$$

$$\Psi_y = \frac{\Phi_y L_y A_y}{M_0} \tag{29}$$

As for the application, it is appropriate to specify the standard mass-flow rate M_0. Thus the non-dimensional group Ψ_x depends on the channel geometry and Ψ_y depends on the header geometry, without considering the flow rates. In cases 1 and 4, the feed flow rates were same, while the dimensions of the header and channel were different, which would have an effect on the two non-dimensional parameters and pressure drop (see Table 2). By increasing the depth of the channel and depth of header from 0.35 to 0.55 mm in our experiments, the total pressure drop decreased from 5.77 to 2.59 kPa, the channel geometry parameter (Ψ_x) decreased from 8.68 to 7.97, and the header geometry parameter (Ψ_y) decreased from 5.51 to 3.78. In order to compare the effect of the two parameters on flow distribution, the calculation results are shown in Fig. 8. It is apparent that the header geometry parameter (Ψ_y) greatly affects the flow distribution in the plate, which will become more uniform when Ψ_y decreases. By contrast, the channel geometry parameter (Ψ_x) nearly has no effect on the flow distribution.

4.4. Effect of the length ratio of manifold opening to header region

In our experiments, the manifold opening length (L_b) is 40 cm, while the total length of the header region (L_y) is 90 cm, thus, the length ratio of manifold opening to header region ($\alpha = L_b/L_y$) is 4/9. To explore this ratio effect on flow distribution, different designs are shown in Fig. 9. When α is increased from 4/9 (see Fig. 9(a)), the

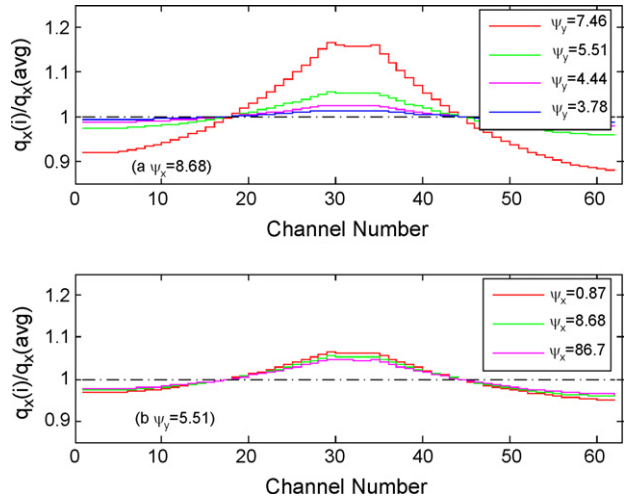

Fig. 8. Compare the effect of two geometrical parameters on the flow distribution respectively, when (a) $\Psi_x = 8.68$ and (b) $\Psi_y = 5.51$.

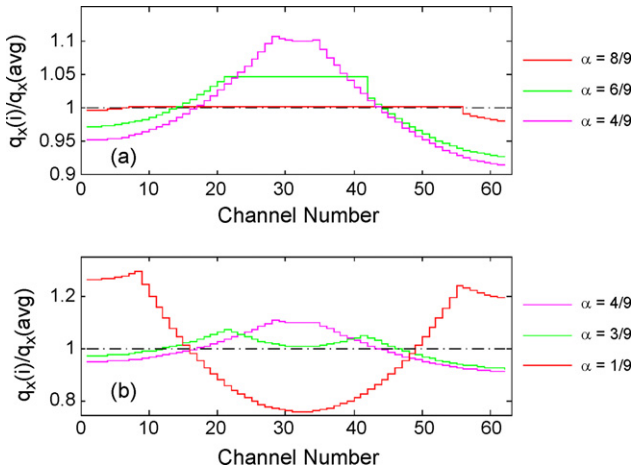

Fig. 9. Effect of the length ratio of manifold opening to header region on flow distribution: (a) $\alpha \geq 4/9$ and (b) $\alpha \geq 4/9$.

channel-flow distribution will become more uniform and the peak value of flow flux usually exists in the center. What is more interesting, the peak will break up to two sharp peaks, when the ratio is decreased from 4/9 (see Fig. 9(b)). In addition, the two peaks will move from the centre to the edge, respectively, and the center will have the lowest volume flow rate. Apparently, the flow distribution will become more uniform if this ratio is higher, however, it's not fit for practical application. Thus there is a contradiction for the flow field design, which needs to be optimized.

4.5. Optimized design for uniform distribution

By analyzing the Eqs. (19) and (29), the hydraulic diameter (D_y) also has effect on the header geometry parameter (Ψ_y), and it will influence the flow distribution greatly as shown in Fig. 10(a). Similar to Eq. (10), the largest D_y will be obtained in a square header, if the perimeter is fixed. In general, the large size and the square cross section of the distribution region will be better for uniform distribution. As illustrated in Fig. 10(b), the proper length ratio of manifold

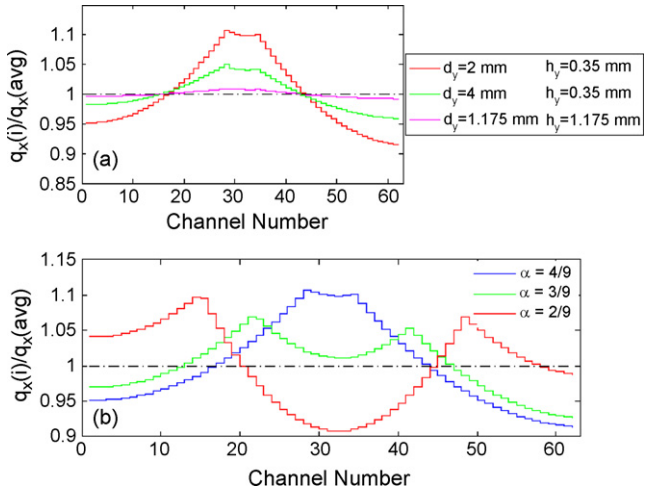

Fig. 10. Comparison of strategy for uniform flow distribution: (a) the geometry aspect effect and (b) the suitable length ratio of manifold opening to header region.

opening to header region is also important for flow distribution. And the opening length, which takes one third of header region, will be fit for both uniform distribution and compact construction in the fuel-cell plate for application.

5. Conclusions

The flow distribution in a parallel-channel plate with the manifold openings is analyzed by the hydrodynamic model, which is also validated by experiments. It's found that the non-uniformity in the flow distribution increases with the feed flow rate. In our experiments, the maximum flow rate usually exists near the centre. The results show that, the header geometry parameter (Ψ_y) usually has great effect on the flow distribution. Thus, in order to get uniform distribution, the large size and the square cross section of the distribution region should be commended. In addition, the effect of the length ratio of manifold opening to header region is also discussed, and 1:3 is considered as the suitable ratio for both uniform distribution and compact construction in the fuel-cell plate for application.

Acknowledgements

This work was supported by the Dalian Sunrise Power Co., Ltd. We gratefully acknowledge the close collaborations with Dalian Sunrise Power Co., Ltd. in the development of full cell applications.

References

[1] Y. Baolian, Fuel Cell—Principle, Technology and Application, vol. 7, Chemical Industry Press (CIP), Beijing, 2003, 160 pp.
[2] R.J. Kee, P. Korada, K. Walters, M. Pavol, J. Power Sources 109 (2002) 148–159.
[3] S. Maharudrayya, S. Jayanti, A.P. Deshpande, J. Power Sources 144 (2005) 94–106.
[4] J.H. Koh, H.K. Seo, C.G. Lee, Y.S. Yoo, H.C. Lim, J. Power Sources 115 (2003) 54–65.
[5] P. Quan, B. Zhou, A. Sobiesiak, Z. Liu, J. Power Sources 152 (2005) 131–145.
[6] S. Maharudrayya, S. Jayanti, A.P. Deshpande, J. Power Sources 138 (2004) 1–13.
[7] A. Kazim, P. Forges, H.T. Liu, Int. J. Energy Res 27 (2003) 401–414.
[8] H.M. Jung, W.Y. Lee, J.S. Park, C.S. Kim, Int. J. Hydrogen Energy 29 (2004) 945–954.
[9] Robert Angelo Mercuri, Seven Hills, US Patent 7,094,311 B2, 2006.
[10] W.M. Kays, M.E. Crawford, Convective Heat and Mass Transfer, McGraw-Hill, New York, 1980.